Available online at www.sciencedirect.com
SCIENCE DIRECT®
Pergamon
Cement and Concrete Research 34 (2004) 1243–1249
CEMENT AND CONCRETE RESEARCH

X-ray absorption fine structure spectroscopy and X-ray diffraction study of cementitious materials derived from coal combustion by-products

S. Pattanaik[a,*], G.P. Huffman[b], S. Sahu[c], R.J. Lee[c]

[a]*Illinois Institute of Technology, Bailey Hall 703, 3101 South Wabash Avenue, Chicago, IL 60616, USA*
[b]*Consortium for Fossil Fuel Science, University of Kentucky, 111 Whalen Building, 533 South Limestone Street, Lexington, KY 40506, USA*
[c]*R.J. Lee Group, 350 Hochberg Road, Monroeville, PA 15146, USA*

Received 24 January 2003; accepted 15 December 2003

Abstract

Cementitious materials derived from coal combustion by-products have been investigated by means of X-ray diffraction (XRD) and S and Ca K-edge X-ray absorption fine structure (XAFS) spectroscopy. The XRD analysis revealed that these materials are a complex mixture of a small amount of quartz [SiO_2] and three calcium-bearing compounds: hannebachite [$CaSO_3 \cdot 1/2H_2O$], gypsum [$CaSO_4 \cdot 2H_2O$] and ettringite [$(Ca_6(Al(OH)_6)_2(SO_4)_3 \cdot 26H_2O)$]. Analysis of the S XAFS data focused on deconvolution of the X-ray absorption near-edge structure (XANES) regions of the spectra. This analysis established that sulfate and sulfite are the two major sulfur forms, with a minor thiophenic component contained in unburned carbon in the fly ash. Increasing sulfate and decreasing sulfite correlated well with increasing gypsum and ettringite and decreasing hannebachite content in the samples. Different calcium compounds were identified primarily through simple comparison of the Ca K-edge XANES and radial structure functions (RSFs) of the cementitious samples with those of reference compounds. Because of the complex coordination chemistry of calcium in these materials, it was difficult to obtain detailed local atomic environment information around calcium beyond the first Ca–O peak. Analysis of the extended X-ray absorption fine structure (EXAFS) and the RSF gave average Ca–O distances in the range 2.44–2.5 Å, with each calcium atom surrounded roughly by eight oxygen atoms. In certain samples, the average Ca–O distances were close to that in ettringite (2.51 Å), suggesting that these samples have higher ettringite content. The results of S and Ca K-edges XAFS and the XRD data were in reasonable agreement.

Keywords: X-ray diffraction; X-ray absorption fine structure (XAFS) spectroscopy; Filler; Ettringite; Coal combustion by-products

1. Introduction

Each year millions of tons of coal combustion by-products (CCBs) are produced by utility power plants in the United States. Furthermore, annual productions of flue gas desulfurization (FGD) by-products continue to increase as the result of stringent sulfur emission restrictions. CCBs contain cementitious materials such as fly ash, bottom ash, boiler slag, and FGD products. The potential commercial uses of CCBs for replacement of cement in concrete, structural fill, road bases, and other construction-related applications have been well documented. However, confusion over the nature of the structural fill highlights the need for detailed characterization of the materials with the goal of setting standards for acceptability of CCBs for use in commercial projects. Samples of cementitious materials derived from CCBs clearly show that the behavior of the materials in an engineered structure changes over time. Much of this change is attributed to the formation of minerals comprised of varying proportions of the FGD constituents. One major concern in compacted FGD fills is that the formation of ettringite and other ettringite-like minerals can cause uncontrollable swelling of the fill, resulting in the loss of structural integrity [1]. Swelling due to ettringite formation is attributed to its needlelike structure. A more recent study on masonry mortar shows that such structural damage may be associated with both ettringite and thaumasite formations [2].

Understanding the structure and properties of cementitious materials presents one of the main challenges in cement chemistry. The variable mineral composition and

* Corresponding author. Tel.: +1-312-225-2683.
E-mail address: sidpattanaik@yahoo.com (S. Pattanaik).

0008-8846/$ – see front matter © 2004 Elsevier Ltd. All rights reserved.
doi:10.1016/j.cemconres.2003.12.017

numerous substitutions that can occur in this material make characterization of such materials difficult. In this regard, X-ray absorption fine structure (XAFS) spectroscopy [3], combined with conventional X-ray diffraction (XRD) techniques, may offer particular advantages in identifying various mineral forms that may be related to structural damage. In the present investigation, a number of cementitious materials and relevant standard compounds have been investigated by combining XAFS spectroscopy and XRD techniques. The S K-edge X-ray absorption near-edge structure (XANES) was particularly useful in quantitatively determining the different molecular forms of sulfur in the materials, while the Ca K-edge XANES and extended X-ray absorption fine structure (EXAFS) were useful in identifying the various Ca minerals present. By comparison of the XANES spectra of cementitious samples with appropriate reference compounds at both edges, identification of various mineral phases as well as oxidation states of both calcium and sulfur in the samples were accomplished. The XAFS results were generally in good agreement with the major mineralogical phases indicated by XRD.

2. Experimental

2.1. Cementitious materials

The samples under investigation were cementitious materials produced by adding materials from a FGD process spray drier to fly ash and about 3 wt.% of lime kiln dust (LKD), and then stabilizing by adding water. These samples were placed in a storage yard or put into application as structural fill for several years (approximately 2–3 years). They were extracted from their respective sites and dried at 60 °C for 12 hours.

2.2. ICP Analysis

The sample was ground to promote efficient processing. The ground sample was ashed to remove free and bound water and organic components, and to convert elements to their oxide phases. The sample was then digested with a sequence of hydrofluoric acid, nitric acid, and Aqua Regia to volatilize the silicon in the form of silicon tetrafluoride and to dissolve and extract the other elements. For most matrices, the final extract should not contain any undissolved residue. The extract was then analyzed by inductively coupled plasma spectrometry (ICP) for the elements of interest. Some partial chemical composition data for the samples are given in Table 1.

2.3. Reference compounds

The ettringite [$(Ca_6(Al(OH)_6)_2(SO_4)_3 \cdot 26H_2O)$] sample was synthesized in our laboratory from calcium hydroxide and aluminum sulfate. Thaumasite [$Ca_3Si((OH)_6(CO_3)(SO_4) \cdot 12H_2O)$] mineral was purchased from Mineralogical Research, California, USA, while hannebachite [$CaSO_3 \cdot 1/2H_2O$] was obtained from a manufacturer who is using this material as filler.

Table 1
Chemical analysis of cementitious samples (wt.%)

Sample ID	pH	Al_2O_3	SiO_2	SO_3	CaO	Fe_2O_3
1	9.72	16.4	46.2	12.7	17.9	3.63
2	9.7	15.9	47.2	12.9	17.2	3.46
3	9.83	ND[a]	ND	16.8	33.5	ND
4	N/A	ND[a]	ND	13.4	23.8	ND
5	9.8	ND[a]	ND	15.6	22.7	ND
6	9.53	ND[a]	ND	7.6	10.6	ND
7	N/A	ND[a]	ND			ND

[a] ND = not determined.

2.4. Powder XRD

The XRD measurements were made according to the following procedure. The material was ground to a fine powder in a ball mill. Approximately 2 g of the powdered material were weighed on a Denver microbalance and loaded into a standard sample holder. Powder XRD patterns were recorded at room temperature by a SIEMENS D-500 diffractometer equipped with a diffracted beam monochromator and a scintillation detector using Cu Kα ($\lambda = 1.5406$ Å) radiation. The data for all samples, including those of reference compounds, were collected in steps of 0.01° in the range 10° 2θ 90° with a counting time of 2 s per step. The data were collected digitally using Visual-XRD from Diffraction Technologies. Quantitative analysis was performed on each sample following the internal standard method reported elsewhere [4]. Standard reference materials were used to derive calibration coefficients for each mineral detected in the samples. The weight percentage of the amorphous component was determined from the integrated intensity of the amorphous "hump" between 20° and 30°.

2.5. XAFS measurements

X-ray absorption measurements at the S and Ca K-edges for the samples listed in Table 1 and the reference compounds described above were made at beamline X-19A at the National Synchrotron Light Source (NSLS), Brookhaven National Laboratory. The samples were appropriately diluted with an inert material, sealed in thin mylar film, and mounted at a 45° angle to the incident X-ray beam for measurement in the fluorescence detection mode employing a Lytle detector. The beam was monochromatized by using a Si(111) double-crystal monochromator, which was detuned to suppress higher harmonics. For the S K-edge (2.472 keV), the data were collected from about 80 eV below the absorption edge to 300 eV above the edge, while the Ca data were collected from about 80 eV below

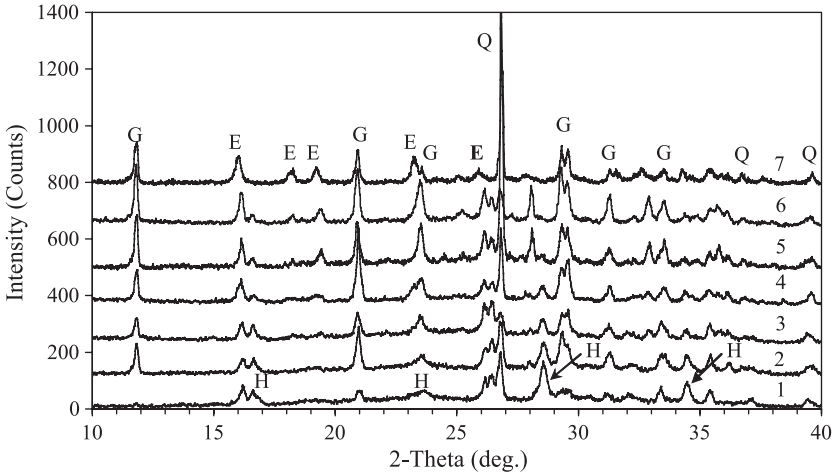

Fig. 1. XRD patterns of cementitious samples. Q = quartz, G = gypsum, H = hannebachite, and T = thaumasite.

the K-edge (4.038 keV) to approximately 750 eV above the edge, which corresponds to a maximum wave vector of 14 $Å^{-1}$.

2.6. Analysis of XAFS Data

Elemental S and calcite were chosen as the primary standards for energy for the S and Ca K-edge spectra. That is, the position of the white line or main peak in the spectrum of elemental S or calcite, $CaCO_3$, was taken as the zero of energy for all S or Ca K-edge spectra, respectively. At least two to three scans were acquired for each sample and added together to improve the signal-to-noise ratio.

The XAFS spectra were analyzed using the software package WinXAS [5]. Standard procedures were followed for background subtraction, normalization, and extraction of EXAFS functions $\chi(k)$ for the Ca K-edge data. The resulting $\chi(k)$ functions were multiplied by a Bessel widow with a window parameter of 2 over a k-range of 1.0–9.0 $Å^{-1}$ and then weighted by k^3 to compensate for the damping of oscillation with increasing k. Fourier transformation of the weighted EXAFS functions gave radial structure functions (RSFs) where well-defined atom–pair interactions could be discerned at various distances. Reliable structural parameters were determined using energy shift and ab initio calculated phase and amplitude parameters from FEFF 7 [6] extracted from the reference compounds. The asymmetry in the Ca–O shell was modeled by r-space fitting using the cumulant expansion method, including third and fourth cumulants, which compensate for phase and amplitude shifts, respectively [7,8]. The shift ΔE_o in the threshold energy was then kept constant at the value refined for a symmetrical distribution, and the coordination number was fixed when the fourth cumulant was refined.

In the case of sulfur, only the XANES spectra were analyzed. This was accomplished by performing least-squares fits of the sample XANES spectra to linear combinations of the XANES of standard compounds.

3. Results and discussion

3.1. XRD analysis

Fig. 1 shows the XRD patterns of all samples listed in Table 1. The samples contain several crystalline phases [quartz (Q), gypsum (G), ettringite (E), thaumasite (T)] as well as an amorphous component. This amorphous component (halo) is attributed to scattering from a glassy aluminosilicate phase, which is commonly found in fly ash [9]. A detailed JCPDS search/match was performed to identify the major crystalline phases that are consistent with various peaks in the diffraction pattern. The peaks at around 27°, 36°, and 39° are assigned to quartz (PDF #48-1045), which appears to be present in all samples. The amount of quartz varies considerably among the various samples. Two peaks

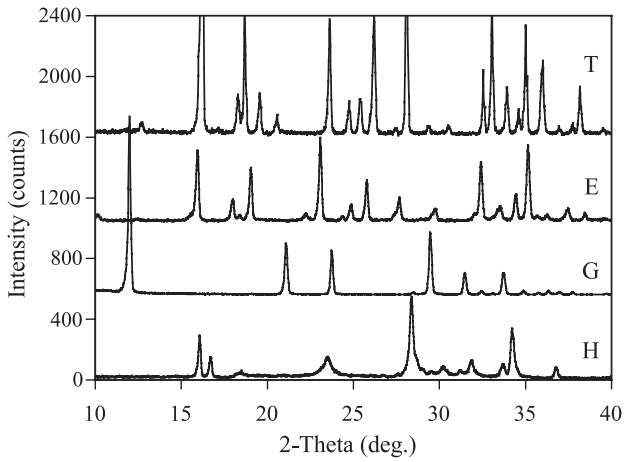

Fig. 2. XRD patterns of hannebachite, gypsum, thaumasite, and ettringite used as internal standards for quantitative analysis.

Table 2
XRD analysis of the cementitious samples with mineral composition expressed in wt.%

Mineral phase	Sample ID						
	1	2	3	4	5	6	7
Hannebachite	17.7	12.4	>0.0	6.8	>0.0	5.5	>0.0
Gypsum	>0.0	5.5	4.6	7.3	9.8	4.0	5.6
Ettringite	>0.0	4.7	15.7	12.8	26.9	8.7	29.7
Quart	3.1	3.1	3.7	2.6	3.5	1.3	9.4
Mull	11.0	11.9	16.8	10.6	11.9	15.4	
Calcite	0.6	1.8	1.8	2.9	3.0	1.5	2.5
Amorphous	37.2	36.2	36.1	36.0	36.9	53.1	30.3
Difference	30.5	24.5	21.4	21.0	8.0	10.5	14.4

at about 23.5° and 28.5° and a doublet at around 16° are indexed as hannebachite (PDF #39-0725). A strong peak at about 12° and three other peaks at 21°, 29°, and 32° arise from gypsum (PDF #21-0816). Since ettringite and thaumasite have similar cell dimensions, they exhibit very similar XRD patterns (see Fig. 2). Thus, it was not immediately clear from XRD whether the peaks at 16°, 18°, 19°, and 23.5° belonged to ettringite (PDF #41-1451), thaumasite (PDF #46-1360), or their combination. However, analysis of the XAFS data gave a clear indication of the presence of ettringite. The results of the XRD analysis are briefly summarized below.

1. Sample 1: Primarily a mixture of hannebachite with a small amount of quartz and gypsum.
2. Samples 2 through 6: Mixtures of hannebachite, quartz, gypsum, and ettringite.
3. Sample 7: Primarily a mixture of ettringite, gypsum, and quartz.

Notice that the intensity of hannebachite peak (16.5°) gradually decreases from Samples 1 through 7, while that of ettringite (16°) and gypsum (12°) increase. This can be interpreted as a transformation of hannebachite to ettringite and gypsum. Such a transformation can occur by reaction of hannebachite with excess alumina and calcium oxide in the presence of an excess of oxygen. Calcite, maghemite, and

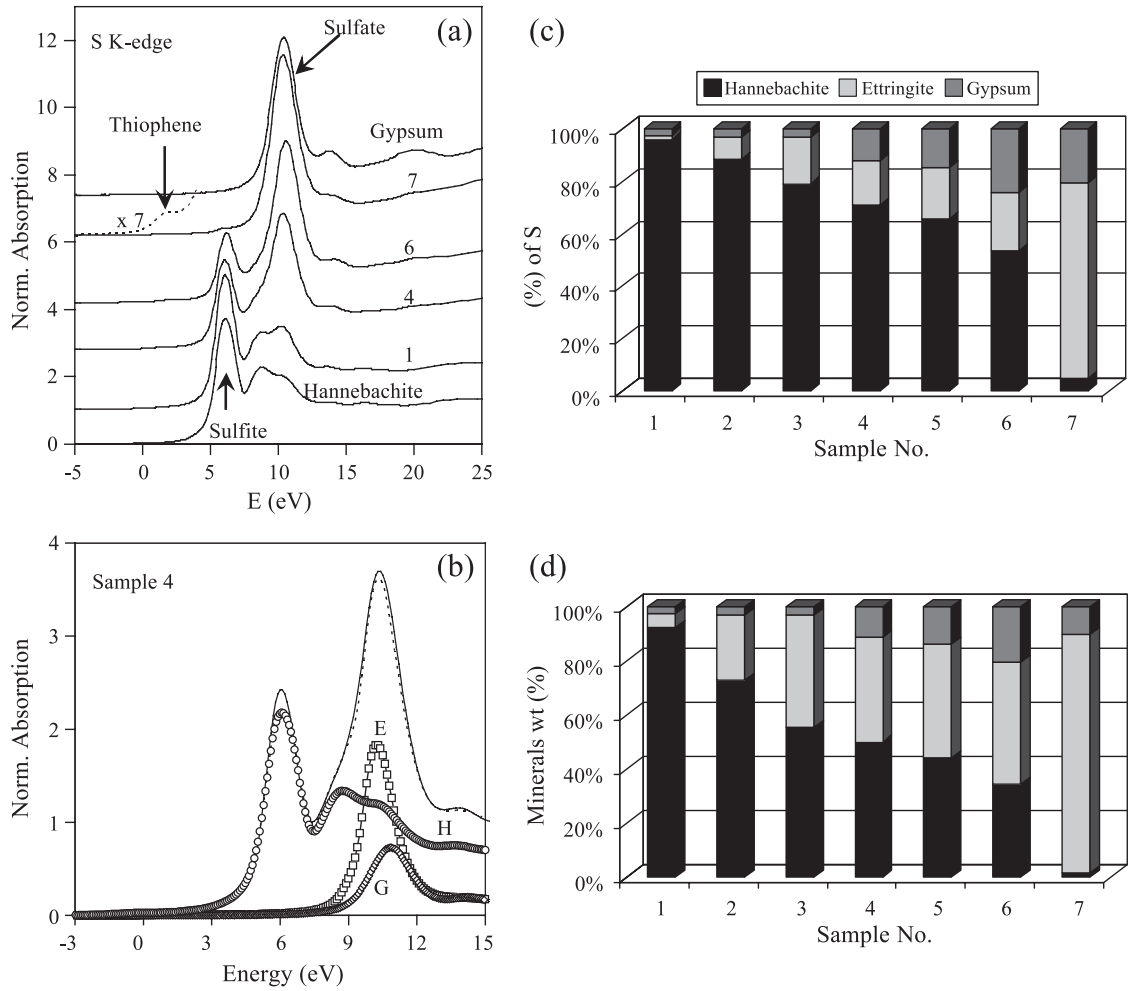

Fig. 3. S K-edge (a) normalized XANES spectra of several cementitious samples compared with reference compounds; (b) speciation of Sample 4 and the probable species derived from the fit; (c) bar diagram indicating the percentages of the total of S contained in different mineral forms; and (d) conversion to wt.% of different minerals in the cementitious samples.

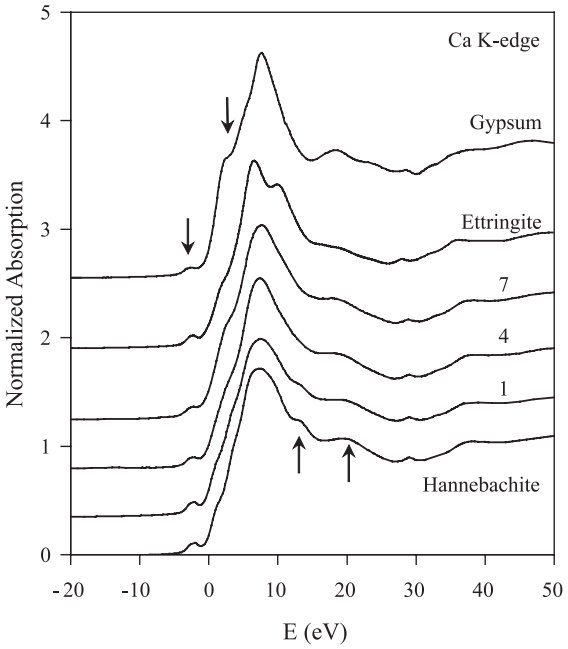

Fig. 4. Normalized Ca K-edge XANES spectra of several cementitious samples compared with reference compounds.

mullite are also present in small amounts, associated with fly ash in the samples [10]. The results of the XRD analysis for the amounts of the various minerals present are presented in Table 2.

3.2. XAFS analysis

3.2.1. S K-edge XANES

Fig. 3a shows the normalized S K-edge XANES spectra of several of the cementitious samples listed in Table 1. Visual inspection and first derivatives of these spectra revealed a set of peaks in the vicinity of the absorption edge: two strong peaks at 6.5 and 10.4 eV, a smaller peak or shoulder at approximately at 8.5 eV, and a very weak peak at about 2.0 eV. Briefly, the peaks observed are of two types: (1) peaks arising from transitions of electrons excited from the sulfur 1s orbital to unoccupied 3p orbitals ($s \rightarrow p$ transitions), and (2) multiple scattering peaks. The positions and intensities of the $s \rightarrow p$ peaks are highly sensitive to the valence states of sulfur and can be used to identify different molecular forms of sulfur [11,12]. A series of plausible S compounds were measured to model and aid quantification of the unknown species in these cementitious samples. The S K-edge spectrum of hannebachite exhibits a main peak at 6.5 eV due to sulfite, which is accompanied by two other peaks at about 8.5 and 10.4 eV. Gypsum and ettringite exhibit a strong peak at 10.0 eV arising from sulfate peak (Fig. 3a). The relative intensity of the sulfite and sulfate peaks varies significantly in the cementitious samples.

The S K-edge sample spectra were analyzed by least-squares fitting to a linear combination of the XANES spectra of hannebachite, ettringite, and gypsum using WinXAS [11,12]. Fig. 3b shows the S K-edge XANES fit and the probable species derived from this fit for Sample 4. The XANES fit gave the percentages of S in different mineral forms (see Fig. 3c), which was then converted to approximate weight percentages of different minerals in each sample (see Fig. 3d). A small amount (< 1 wt.%) of thiophenic sulfur (not shown) was also detected in most samples. As expected, weight percent of various sulfur compounds from XANES differ from those reported from XRD. The weight percent from XRD was calculated taking into account all the phases including the amorphous com-

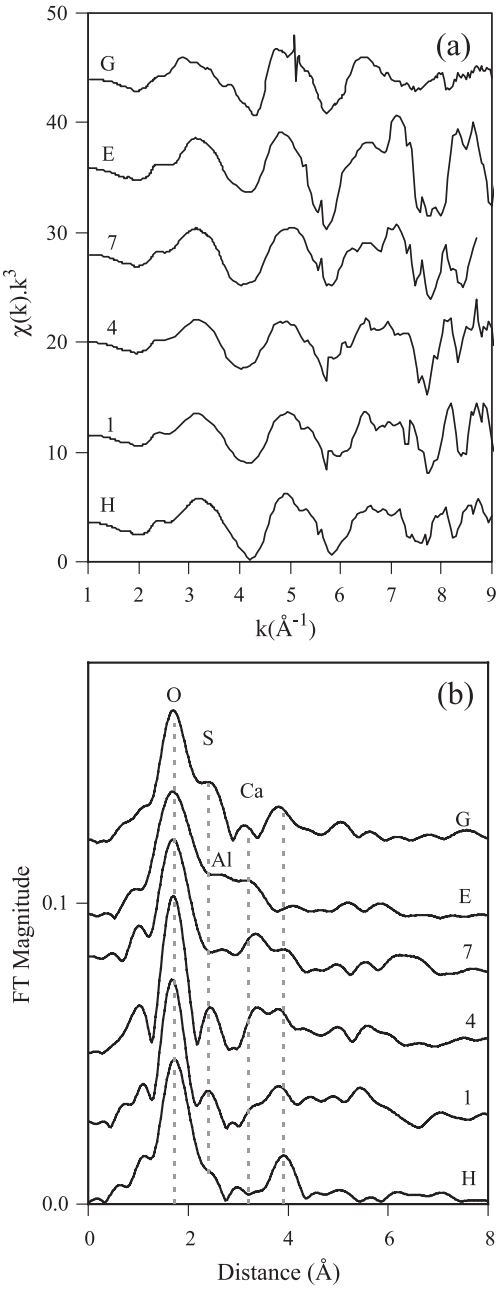

Fig. 5. Ca K-edge (a) weighted EXAFS functions and (b) radial structure functions of several cementitious samples and reference compounds.

ponent in a given sample as opposed to XANES calculation based on only sulfur compounds.

3.2.2. Ca K-edge XAFS

Fig. 4 illustrates the normalized Ca K-edge XANES of several cementitious samples and reference compounds. The XANES spectra of both Samples 1 and 2 closely resemble hannabachite, suggesting that hannabachite is a major component in these two samples. Such resemblance can also be seen in their S K-edge XANES and XRD data. As we go from Sample 1 to Sample 7, the XANES spectrum approaches that of gypsum, with the dominant peak or "white line" at about 7 eV becoming sharper, and the peak at 20 eV shifting gradually towards lower energy. This coincides with the trend of increasing gypsum and ettringite with decreasing hannebachite content shown by the S XANES data. Additionally, the main peak of Sample 7 is wider than that of the other samples because it contains more ettringite than any other sample, which is in agreement with both XRD and S K-edge XANES.

3.3. Ca K-edge EXAFS and RSFs

The RSFs represent the local atomic environment around the probe atom. They are obtained by Fourier transformation of the weighted EXAFS function, $k^3\chi(k)$ [7]. Figs. 5a and b compare the Ca K-edge EXAFS and RSF of several cementitious samples with those of the model compounds. As discussed earlier, XRD and S K-edge XANES indicated that these cementitious samples contain three Ca compounds, hannebachite, gypsum, and ettringite. Consequently, the RSF, shown in Fig. 5b, should be a linear combination of the signals from those different environments and it is difficult to obtain any detailed local atomic environment information about Ca through direct analysis of the RSF, with the exception of the first Ca–O shell. The Ca–O, Ca–S, Ca–Al, and Ca–Ca bond distances and coordination numbers for several reference compounds are summarized in Table 3. The dashed lines in the RSF (Fig. 5b) indicate the positions of the peaks representing the O, S, Al, and Ca shells surrounding the absorbing Ca atom in these compounds. In Samples 1–4 the Ca–S peak appears at about same position as in gypsum (3.14 Å) [13] and hannebachite (3.27 Å) [14], suggesting that Samples 1 and 4 contain both these compounds. In Sample 7, on the other hand, this peak has shifted towards a higher distance and corresponds to a Ca–Al interaction as in ettringite (3.43 Å) [15]. A single peak at about 3.8 Å represents the Ca–Ca interaction in gypsum and hannebachite while it is at 3.6 Å for ettringite. This peak is split into two in Samples 4 and 7, which is expected if these samples were a mixture of ettringite, hannebachite, and gypsum. The Ca–Ca distances in these reference compounds are 3.72, 3.96, and 4.06 Å, respectively, with a coordination number of 2 (see Table 3). The real space refinement of the Ca–O shell was performed in the range 1.2–2.2 Å. The results of least-squares refinement are summarized in Table 3 and are compared with the structural parameters of relevant reference compounds. The average Ca–O distances in hannebachite, gypsum, and ettringite are 2.44, 2.45, and 2.51 Å. For cementitious samples, the refinement gave an average Ca–O distance of 2.47 Å for Sample 1, which is closer to that of hannebachite and gypsum, indicating that Sample 1 contains these two compounds. In both Samples 4 and 5, the Ca–O distance is 2.5 Å, which is close to that of ettringite, indicating more ettringite in these samples. The data for Samples 6 and 7 were not good enough to be able to correlate the Ca–O bond distance to specific compounds. Not surprisingly, Ca is coordinated to eight oxygen atoms in all samples.

Table 3
Relevant structural parameters for cementitious materials and model compounds derived from EXAFS and values for the model compounds from XRD

Sample	Bond	d/Å	σ^2/Å^2	N	ΔE_o/eV
1	Ca–O	2.47	0.008	8	−8.1
2	Ca–O	2.44	0.01	8	−8.1
3	Ca–O	2.49	0.006	8	−8.1
4	Ca–O	2.50	0.007	8	−8.1
5	Ca–O	2.50	0.003	8	−8.1
Gypsum	Ca–O	2.46		8	XRD
	Ca–S	3.14		2	
	Ca–Ca	4.06		2	
Hannebachite	Ca–O[a]	2.44	0.002	8	−8.1
	Ca–O	2.43		8	XRD [14]
	Ca–S	3.27		2	
	Ca–Ca	3.96		3	
Ettringite	Ca–O	2.51		8	XRD [15]
	Ca–Al	3.43		4	
	Ca–Ca	3.72		4	
	Ca–S	>5.4		2	
Thaumasite	Ca–O	2.45		8	XRD [16]
	Ca–Si	3.42		2	
	Ca–Ca	3.84		2	

d is the distance, N is the coordination number, σ^2 is the Debye–Waller factor, ΔE_o is the difference in threshold energy shift, $S_o^2 = 0.7$; ΔR/Å = 1.0–2.20.

[a] Structural parameters are derived from EXAFS.

4. Conclusions

XAFS spectroscopy provides a quantitative estimation of the amount of sulfate and sulfite present in cementitious samples. Sulfur is predominantly present as a sulfite in the mineral hannebachite and as a sulfate in the minerals ettringite and gypsum. By least-squares analysis of the S XANES spectra, a quantitative analysis of the amounts of these three minerals in cementitious material may be performed. The results obtained by XRD analysis of the samples are consistent with the S XANES analysis, as are the trends observed in the Ca XANES spectra and RSF. The average Ca–O distances lie in the range 2.44–2.50 Å, and the variation of Ca–O distances is consistent with the mineral percentages in the respective samples. These results

indicate that a combination S and Ca K-edge XAFS spectroscopy and XRD provides a new method for quantitative analysis of phases in cementitious materials that are of significant concern with regard to the structural integrity of compacted FGD fills.

Acknowledgements

We gratefully acknowledge the use of beamline X-19A at the National Synchrotron Light Source, Brookhaven National Laboratory, which is supported by the U.S. Department of Energy (U.S. DOE). We also thank Henry Francis of the Kentucky Geological Survey for assistance with the XRD analysis and Prof. Frank E. Huggins of the University of Kentucky for assistance with the XAFS measurements.

References

[1] R.J. Lee, W.E. Wolfe, T.S. Butalia, The effect of ettringite formation on the expansion properties of a compacted spray dryer ash fill, 2001 International Ash Utilization Symposium (October 2001) 22–24.

[2] M.E. Gaze, N.J. Crammond, The formation of thaumasite in a cement:lime:sand mortar exposed to cold magnesium and potassium sulfate solutions, Cem. Concr. Compos. 22 (2000) 209–222.

[3] R.J. Kirkpatrick, G.E. Brown, N. Xu, X. Cong, Ca X-ray absorption spectroscopy of C-S-H and some model compounds, Adv. Cem. Res. 9 (1997) 31–36.

[4] G.J. McCarthy, A. Thedchanamoorthy, Semi-quantitative analysis of fly ash by the reference intensity ratio method in fly ash coal conversion by-products: Characterization, utilization and disposal V, Mater. Res. Soc. Symp. Proc. 136.

[5] T. Ressler, WinXAS: A program for X-ray absorption spectroscopy data analysis under MS-Windows, J. Synchrotron Radiat. 5 (1998) 118–122.

[6] S.I. Zabinsky, J.J. Rehr, A. Aukudinov, FEFF code for ab initio calculation of XAFS. PhD thesis, University of Washington, 1996.

[7] E.D. Crozier, J.J. Rehr, R. Ingalls, Amorphous and liquid systems, in: D.C. Koningsberger, R. Prins (Eds.), X-ray Absorption Principles, Applications, Techniques of EXAFS, SEXAFS and XANES, Wiley-Interscience, New York, 1988, pp. 373–442.

[8] D.S. Yang, D.R. Fazzini, T.I. Morrison, L. Tröger, G. Bunker, Modeling of pair distribution functions for XAFS in disordered systems, Nucl. Instrum. Methods 210 (1997) 275–286.

[9] G.P. Huffman, A.D. Shah, N. Shah, J. Zhao, F.E. Huggins, J.J. Helble, S. Srinivasachar, T.W. Peterson, J.O.L. Wendt, N. Gallagher, L.E. Bool, A. Sarofim, The impact of ash deposition on coal fired plants, in: J. Williamson, F. Wigley (Eds.), Proceedings of the Engineering Foundation Conference (1993), Birmingham, UK, Taylor & Francis, London, 1994, pp. 409–423.

[10] A. Palomo, M.W. Grutzeck, M.T. Blanco, Alkali-activated fly ashes: A cement for the future, Cem. Concr. Res. 29 (1999) 1323–1329.

[11] G.P. Huffman, S. Mitra, F.E. Huggins, N. Shah, S. Vaidya, F. Lu, Quantitative analysis of all major forms of sulfur in coal by X-ray absorption fine structure spectroscopy, Energy Fuels 5 (1991) 574–581.

[12] M.M. Taghiei, F.E. Huggins, N. Shah, G.P. Huffman, In situ X-ray absorption fine structure spectroscopy investigation of sulfur functional groups in coal during pyrolysis and oxidation, Energy Fuels 6 (1992) 293–300.

[13] W.F. Cole, C.J. Lancucki, A refinement of the crystal structure of gypsum CaSO4·2(H_2O), Acta Cryst. B30 (1974) 921–929.

[14] T. Matsuno, H. Takayanagi, K. Furuhata, M. Koishi, H. Ogura, The crystal structure of calcium sulfite hemihydrate, Bull. Chem. Soc. Jpn. 57 (1984) 1155–1156.

[15] A.E. Moore, H.F.W. Taylor, Crystal structure of ettringite, Acta Cryst. B26 (1970) 386–393.

[16] H. Effenberger, A. Kirfel, G. Will, E. Zobetz, A further refinement of the crystal structure of thaumasite, $Ca_3Si(OH)_6(CO_3)(SO_4)\cdot 12H_2O$, Neues Jahrb. Mineral. Monatsh. 1983 (1983) 60–68.